Structural and textural features of TiO$_2$/SAPO-34 nanocomposite prepared by sol-gel method

Salima Bellatreche [a], Abdelkrim Hasnaoui [a], Bouhadjar Boukoussa [a,b,*], Jaime García-Aguilar [c], Ángel Berenguer-Murcia [c], Diego Cazorla-Amoros [c], Abdelkader Bengueddach [a].

[a] Laboratoire de Chimie des Matériaux L.C.M, Université d'Oran1 Ahmed Benbella, BP 1524 El-Mnaouer, 31000 Oran, Algeria

[b] Université des Sciences et de la Technologie Mohamed Boudiaf, Faculté de Chimie, Département de Génie des Matériaux, BP 1505, Oran El-Mnaouer, Algeria

[c] Inorganic Chemistry Department and Materials Science Institute, Alicante University, Ap. 99, E-03080 Alicante, Spain.

* Corresponding author. Tel.: +213771663458, E-mail addresses: bbouhdjer@yahoo.fr

Abstract

This paper focuses on the synthesis of nanocomposite materials TiO$_2$/SAPO-34 using the sol-gel method, which involves preparing a mixture between as-synthesized or calcined SAPO-34 zeolite and TiO$_2$ gel under hydrothermal crystallization and then calcined at 400 °C for the formation of TiO$_2$ anatase phase. The structural and textural features of the obtained materials were determined by various physico-chemical techniques such as thermogravimetric analysis (TGA), X-ray diffraction (XRD), scanning electronic microscopy (SEM), Nitrogen sorption at 77 K, energy dispersive X-ray analysis (EDX) and ultraviolet-visible (UV-vis). The DRX results showed that calcination at 400 °C of the mixture between calcined SAPO-34 and TiO$_2$ gel led to the collapse of the original framework of zeolite but forms the anatase TiO$_2$ in a nano-spherical morphology, but the use of as-synthesized SAPO-34 supports provides a mixture phase between SAPO-34 and TiO$_2$ anatase after calcination. The photocatalytic properties of SAPO-34/TiO$_2$ and TiO$_2$ type materials were tested for the removal of methylene blue (MB) dye. The MB degradation proved to be increasing as a function of contact time, catalyst mass and the initial concentration of MB.

Keywords: TiO$_2$, SAPO-34, TiO$_2$/zeolite, sol-gel preparation. Methylene blue, Photocatalysis

1. Introduction

Titanium dioxide is classified among the most important semiconductor materials [1,2]. TiO$_2$ is chemically inert [3], thermally stable [4], inexpensive [5], and environmentally friendly [6]. It is used in cosmetics, paint industry, or photocatalysis for degradation of pollutants in contaminated water [7]. All these properties

expanded the field of application of TiO_2 [8-12]. Recently several methods were investigated for the purpose to obtain TiO_2 in the shape of micro and nanoparticles with different morphologies such as nanotubes [13], nanofibers [14], or spheres [15]. Moreover, pure TiO_2 nanoparticles are difficult to be recycled and rapidly lose their effective surface area during their catalytic applications [16,17]. Consequently immobilization of TiO_2 nanoparticles on a support has been proposed to improve their properties [18]. To date, several methods have been employed for the synthesis of composite materials containing TiO_2 including, chemical bath deposition [19], one-step electrochemical anodizing [20], solvent-free in situ synthesis [21], peroxo assisted hydrothermal [22], chemical solvent and chemical vapour decomposition (CSD & CVD) [23,24], precipitation [25] sol-gel method [26] and other methods…

The sol-gel method is the most effective approach which permits to obtain particles in the nano-scale of high purity at relatively low temperature, possibility of stoichiometry controlling process [26]. The materials containing TiO_2 obtained by this method can be re-used for several cycles due to their ease of separation in the reaction medium and its interesting photocatalytic properties. In order to improve these properties, several attempts have been proposed for the immobilization of TiO_2 on different supports such as clay [27], silica's [28], polymer [29], activated carbon [30], zeolite [31]…

Zeolites are interesting support materials due to their high surface area, uniform pores, unique structures, an excellent adsorption and high thermal stability [32]. To date several zeolites have been used as supports for TiO_2 particles such as ZSM-11 [32], Beta [33], Y and X zeolite [34,35], and natural zeolites [36,37]. In general the increase of the calcination temperature leads to the transformation of amorphous TiO_2 to the anatase or rutile phase [36], but for the preparation of composite TiO_2/zeolite it is possible to destroy the original framework of the support [37], due to the thermal dehydration of zeolites [37-39]. The disorder of the zeolite framework also causes a decrease in the crystallinity of zeolite, this phenomenon has already been observed on different types of zeolites [40]. The works of Sun et al have demonstrated that the increase of temperature of calcination does not only affect the zeolite framework but also affects the adsorption behavior and photocatalytic [37].

SAPO-34 is a silicoaluminophosphate has a small pore size ($\sim$3.8 Å) with a chabazite structure containing the composition $Si_xAl_yP_zO_2$ where x=0.01–0.98, y=0.01–0.60, and z=0.01–0.52 [40]. These solids have been

used in the selective catalytic reduction of NOx by ammonia, or the selective conversion of methanol to gasoline, olefins or dimethyl ethers [41,42], they have known a wide application in the field of adsorption of pollutants organic compounds [43,44].

To the best of our knowledge, no attention has been paid to the silicoaluminophosphate SAPO-34 combined with TiO_2. In the present investigation, this innovative concept will be extended to synthesis of composite TiO_2/SAPO-34 using sol gel method. In order to obtain an efficient photocatalyst, easy separation of photocatalyst in the reaction medium, we propose to use the as-synthesized and calcined zeolite SAPO-34 as support for TiO_2. The obtained solids were evaluated as photocatalysts for the degradation of methylene blue (MB). The effect of various parameters such as contact time, catalyst mass and initial dye concentration was investigated.

2. Experimental

2.1. Synthesis of SAPO-34

SAPO-34 was synthesized hydrothermally from a gel with starting molar composition 1 Al_2O_3: 1 P_2O_5: 2.09 Morpholine: 1.08 SiO_2: 66 H_2O according to the literature [45]. The sources for Al, P and Si are, aluminium isopropoxide (89% Prolab) or (Pseudo-bohemite, Pural SBI 75.3% Al_2O_3, 24.7% H_2O), phosphoric acid (85%, MERCK) and fumed silica (Aerosil 200, Degussa) respectively. The mixture was prepared by successive additions of phosphoric acid and morpholine to the suspension of aluminium isopropoxide in water under vigorous stirring. The obtained gel was sealed into a Teflon-lined stainless steel autoclave followed by crystallization for 24 hours at 200 °C. The obtained product was then removed from the oven and cooled to room temperature. After filtration and washing several times with distilled water, the obtained solid was dried at 90°C for at least 24 h. The powder was then calcined in air at 400°C for 6 h to remove the organic products.

2.2. Synthesis of TiO_2

Adapting a synthetic protocol from the literature [46], a quantity of tetrabutylorthotitanate was mixed with 2-butanol and H_2O, the obtained mixture with a composition of 10.03 TBOT: 1.08 butanol: 0.16 H_2O was stirred for 4 hours. The formed gel was filtered, washed, and dried at 90 °C followed by calcination at 400

°C for 12 hours to transform the amorphous gel into the crystalline anatase phase. This composition leads to the production of 0.8 g of anatase TiO_2.

2.3. Sol-Gel synthesis of TiO₂/SAPO-34

The synthesis of composite TiO_2/SAPO-34 involves the preparation of TiO_2 gel using the same composition mentioned previously (see protocol of preparation of TiO_2). For the preparation of 50% TiO_2/SAPO-34 composite, the gel of TiO_2 was added with 0.8 g of SAPO-34 zeolite calcined or as-synthesized, followed by stirring for 1 hour, the formed product was washed, filtered, dried, and calcined at 400 °C for 12 hours.

2.4. Characterization

The silico-alumino-phosphate molecular sieves were characterized by XRD, using a 2002 Seifert powder diffractometer with Cu-Kα radiation (λ=1.54Å) from 15 to 80° at a scanning speed of 2°/min. the diffractometer use a θ-2θ assembly and analyze the samples is powder form (finely grounded) with a flat plate sample holder. The morphology, texture, and homogeneity of the materials were assessed by the analysis of different sections of the samples by scanning electron microscopy coupled to energy dispersive X-ray spectroscopy (SEM–EDX, Hitachi S3000N). The textural characterisation of the catalysts was carried out by means of adsorption of N_2 at −196 °C (Autosorb 6, Quantachrome). Prior to the adsorption measurements, the catalysts were outgassed under vacuum (10^{-2} mbar) at 250 °C for 4 h to remove any adsorbed impurities. Surface area was calculated from the nitrogen adsorption isotherms using the BET equation (S_{BET}) and micropore volume from the DR method. Thermogravimetric analysis (TGA) experiments were performed in a Thermogravimetric Analyzer (TA Instruments, model SDT 2960). In these experiments, approximately 10 mg of the catalyst (fresh and used) were treated. The catalyst was heated up to 900 °C (heating rate of 10 °C/min) and equilibrated for 1 h, under synthetic air (100 ml/min). The SPECORD 210 PLUS UV-Vis spectrophotometer (Analytik Jena) with holmium oxide filter is used for the study of optical properties of obtained materials, optics: Monochromator with holographic concave grating light split into two beams by a beam-splitting plate, wavelength range: 190-1100 nm.

2.5. Photocatalytic degradation of MB

The photocatalytic degradation of MB in catalyst suspensions was performed in a photoreactor. A lamp was located at the top of a 500 ml beaker at a distance of 15 cm. The radiation source was a mercury UV lamp

1115 (25W, 18mA) operating at a wavelength of 254 nm. Prior to illumination, the suspension containing different masses of catalyst (m_1= 0.025g, m_2= 0.1g, m_3= 0.175g, m_4= 0.25g) and 100 mL of MB with different initial concentration 15ppm, 20ppm, 30ppm, 40ppm was stirred for 30 min with a magnetic stirrer in the dark, a 30 min contact time was sufficient for MB to reach adsorption–desorption equilibrium with the catalysts. Then the suspension was irradiated under continuous stirring. At specific time intervals, samples were withdrawn and centrifuged at 4000 rpm to separate the catalyst particles. The concentrations of MB in supernatant were determined by using an UV–visible spectrophotometer (Specord 210 Analytik Jena) registering the absorbance at 660 nm, corresponding to the maximum absorption wavelength of MB. All measurements were performed in triplicate with errors below 5% and average values were reported. The degradation percentage is calculated by the following equation:

$$\tau \% = \frac{C_0 - C}{C_0} \times 100$$

C_0: the initial concentration

C: the concentration at a specific time

3. Results and discussion

Fig. 1a shows the X-ray diffraction patterns of the three samples. The as-synthesized SAPO-34 shows the most intense reflections characteristic of the chabazite (CHA) structure for pure SAPO-34 (2θ = 9.42, 12.77, 15.92, 17.8, 20.5, 24.9, 27.54and 29.49°), that correspond to the following Miller indexes: (101), (110), (021), (003), (211), (104), (131) and (321). All the diffraction peaks are in good agreement with the standard crystallographic data (JCPDS-no. 00-47-0429) reported for SAPO-34. In the case of TiO_2 particles the XRD results showed that the pure anatase phase was obtained after calcinations, with the appearance of all characteristic peaks 2Θ: 25.3, 37.8, 48.0, 54,54.9, 62.7, 68.7 and 75.1 that correspond to the following Miller indexes: (101), (004), (200), (105), (211), (204), (116), (220) and (215) (Fig. 1a). These results are in agreement with the standard crystallographic data (JCPDS-no. 01-086-1157) for anatase TiO_2. In the case of the composite TiO_2/SAPO-34 obtained by as-synthesized SAPO-34, the XRD results (Fig. 1a) show that the composite material was successfully obtained with the occurrence of the characteristic peaks of TiO_2 anatase phase and CHA of SAPO-34. We also showed that there was a decrease in the intensity of the peaks of the

composite material which is due to the calcination procedure. Similar results have been obtained using zeolitic supports when increasing the calcination temperature in the 300-500°C range [37]. This decrease in intensity also may be due to interactions between the precursor of TiO_2 and SAPO-34 support.

It can be seen that the characteristic diffraction lines of TiO_2 are weaker which confirms that TiO_2 is well dispersed on the SAPO-34 zeolite, which prevents the formation of large TiO_2 crystals in the composite materials, as it has been observed previously by Suárez et al. [47].

We have used the Scherrer equation $\left(D = \frac{K\lambda}{\beta cos\theta}\right)$ to determine the mean crystallite sizes of our materials. Where λ is the wavelength of the X-ray, k is a constant $k \approx 0.9$, θ is the diffracting angle, and β is the full width of diffraction peak at half maximum intensity (FWHM). The results shows that the crystallite size increases in the following order 21.04, 27.02 and 28.1nm for TiO_2, SAPO-34 and TiO_2/SAPO-34 composite respectively.

Fig. 1b shows the X-ray diffraction patterns of the composite TiO_2/SAPO-34 prepared by calcined SAPO-34 zeolite (Fig. 1b). We note that the TiO_2/SAPO-34 composite present all the characteristic peaks of the TiO_2 anatse phase. However, any characteristic peak of zeolite SAPO-34 was obtained. In the range $2\theta = 10\text{-}40°$, we observe a broad peak characteristic to the presence of amorphous species confirming the total collapse of the zeolite SAPO-34.

In order to confirm the stability of the SAPO-34 zeolite we have calcined the sample in two successive procedures. Practically no loss in crystallinity was observed when the as-synthesized SAPO-34 were calcined for the first time at 400°C, confirming their thermal stability under calcination conditions (Fig. 1c). However, the XRD result shows that after the second calcination at 400°C the structure of SAPO-34 is collapsed completely (Fig. 1c).

This behaviour with the temperature of calcination, shows that the SAPO-34 does not resist to the effect of re-calcination which is strongly related to the Si–O–Al and P–O–Al bonds opening [48,49]. Whereas, Briend et al showed that the structure of SAPO-34 zeolite deteriorated rapidly when exposed to moisture at low temperatures [50].
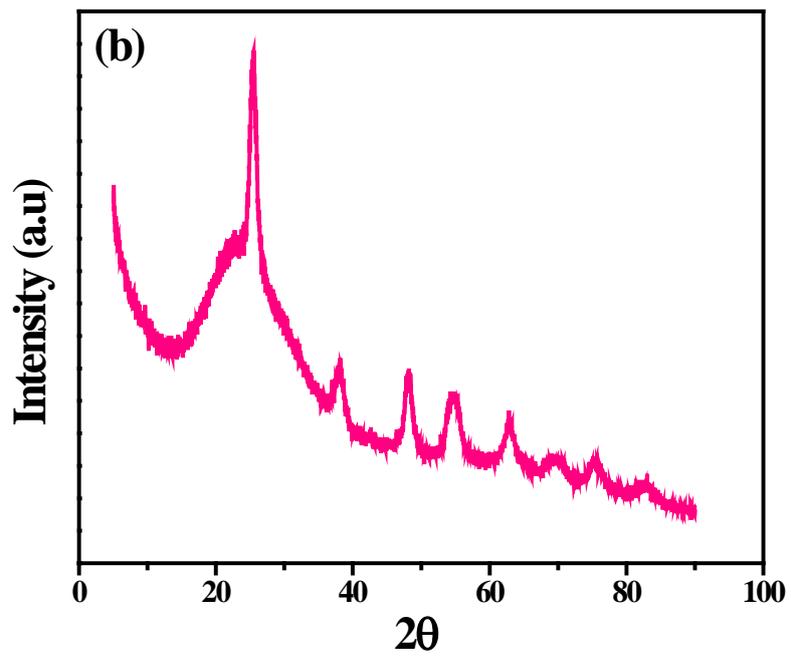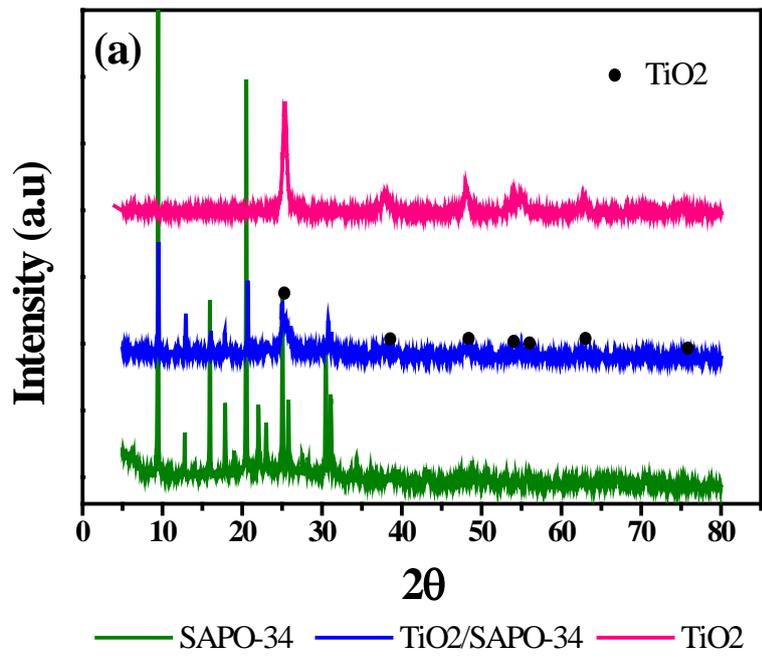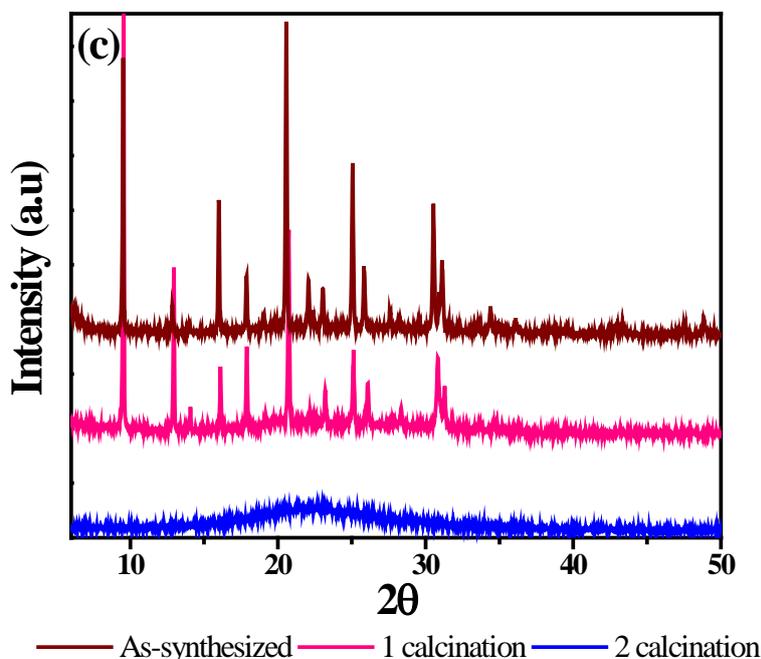
Fig.1. Powder XRD patterns for TiO$_2$, SAPO-34 zeolite and composite TiO$_2$/SAPO-34; (a) TiO$_2$ calcined at 400°C, as-synthesized SAPO-34 and TiO$_2$/SAPO-34 prepared with as-synthesized SAPO-34, (b) TiO$_2$/SAPO-34 obtained by calcined SAPO-34; (c) as-synthesized SAPO-34 calcined in two successive stages at 400 °C.

Fig.2 shows the SEM images of different synthesized materials. The composite TiO$_2$/SAPO-34 prepared with as-synthesized SAPO-34 presents a mixture of morphology between aggregates of TiO$_2$ nanoparticles and the cubic crystals of the SAPO-34 (Fig.2a), it also shows that the TiO$_2$ particles are well dispersed on the surface of zeolite SAPO-34 which are in agreement with the XRD results. According to the SEM images we note that the size of SAPO-34 particles are in the range 6.5-5um, while the TiO$_2$ particles are around 0.5um. In the case of the TiO$_2$/SAPO-34 composite prepared using the calcined zeolite, we observe the spherical morphology which corresponds to the TiO$_2$ anatase with particles sizes around 0.6-0.4 um (Fig.2c). We also note the appearance of particles with different morphologies that are characteristic to the amorphous phase. These results confirm the results obtained by XRD analysis. For the case of SAPO-34 zeolite, a cubic structure is obtained with particles size in the range 4-10 um which characterizes this type of zeolite (Fig.2c). The TiO$_2$ anatase forms agglomerates with the appearance of small crystallites with sizes in the range of a few tens of nanometers (Fig.2d).
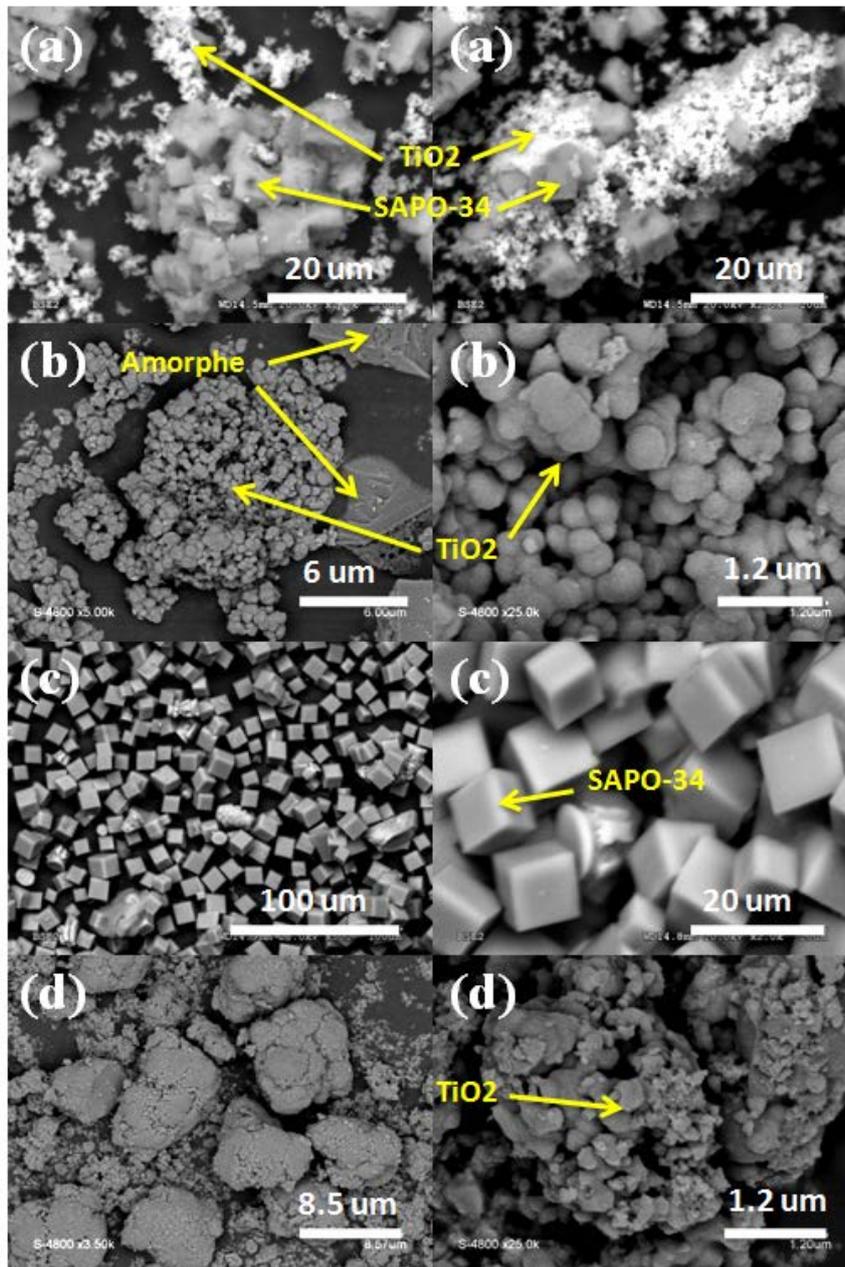
Fig.2. SEM images (a) TiO$_2$/SAPO-34 (using as-synthesized zeolite), (b) TiO$_2$/SAPO-34 (using calcined zeolite), (c) SAPO-34 and (d) TiO$_2$ anatase.

Thermogravimetric analyses (TGA) were investigated to determine the thermal stability of the obtained materials and also for know their states at 400 °C (at the temperature of calcination) (Fig.3). The conventional TiO$_2$ showed a weight loss of 25%, which was attributed to the loss of water and 2-butanol. For the case of SAPO-34 zeolite and TiO$_2$/SAPO-34 composite, the TGA signal of the zeolite is identical to those obtained in the literature [51, 52]. It is clear that the weight loss stages of TiO$_2$/SAPO-34 are different compared to the SAPO-34, which is probably due to the presence of TiO$_2$ nanostructures on the surface of SAPO-34. For both materials, the TGA curve showed four weight-loss steps, the first step which occurred at

temperatures lower than 180°C with weight loss 5% and 8% for SAPO-34 and TiO_2/SAPO-34 respectively, that were attributed to physisorbed and occluded water in the SAPO-34 framework [52], and the remaining three stages are in the range 180-720°C that are attributed to the oxidative decomposition of template [52] (Fig.3), the weight losses in this temperature interval are 19% and 14.5% for SAPO-34 and TiO_2/SAPO-34 respectively.

We can see that the elimination of the structuring agent (morpholine) requires high temperatures (>500 °C), that shows the stability of the zeolite matrix containing the template. We can conclude that the TiO_2/SAPO-34 composite has approximately 60% of organic template decomposed at 400 °C, confirming that the calcination at 400 °C leads to the formation of TiO_2 anatase (see XRD results) and partial calcination of the SAPO-34 zeolite.
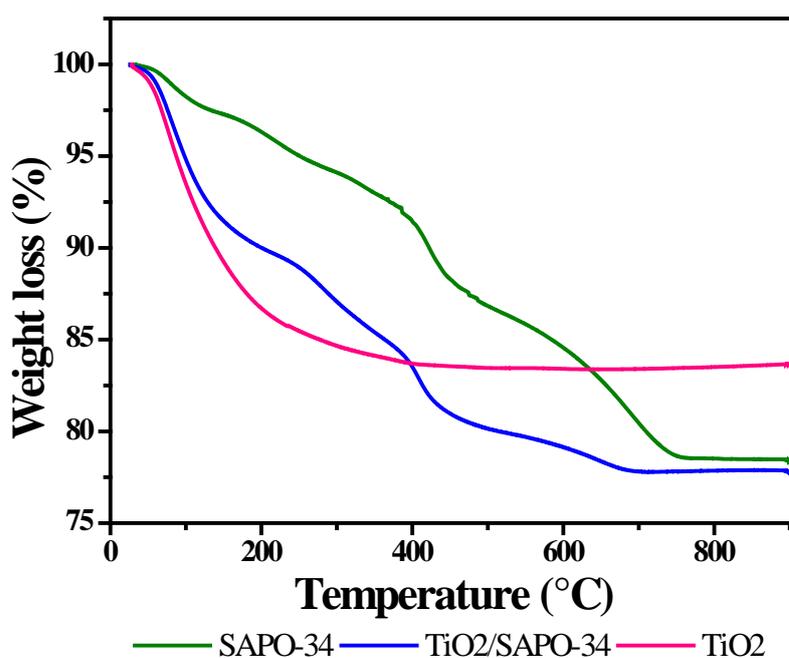

Fig.3. TGA of TiO_2 anatase, as-synthesized SAPO-34 and TiO_2/SAPO-34 using as-synthesized SAPO-34.

Fig.4 shows the nitrogen adsorption–desorption isotherms of the different solids. The SAPO-34 sample show a type I isotherm, typical of microporous solids [41] and exhibit a distinctive hysteresis loop in the higher relative pressure (P/P_0) range of 0.8–1.0, similar to H3 type according to the IUPAC classification [53]. However, the TiO_2 and TiO_2/SAPO-34 composite recovered after calcination exhibit a type IV

isotherm, characteristic of mesoporous materials, While these both materials exhibit hysteresis loops type H3, The surface areas (determined by the BET method) and micropore volume (determined by DR method) of SAPO-34 are found to be the largest among all the samples and decrease when mixing TiO_2 with SAPO-34 support. We note that the TiO_2 nanocrystals have a large pore diameter that corresponds to mesoporous materials (Table1). The BET surface area of TiO_2 anatase is found to be 83 m^2g^{-1} that is higher than TiO_2–P25 (50 m^2g^{-1}). However, we note that the mesopore diameter of the composite materials has decreased compared to TiO_2 nanocrystals, which may be is due to the interaction of these nanoparticles with the SAPO-34 surface that reduces the interparticle space of TiO_2 nanoparticles responsible of the mesoporosity observed.
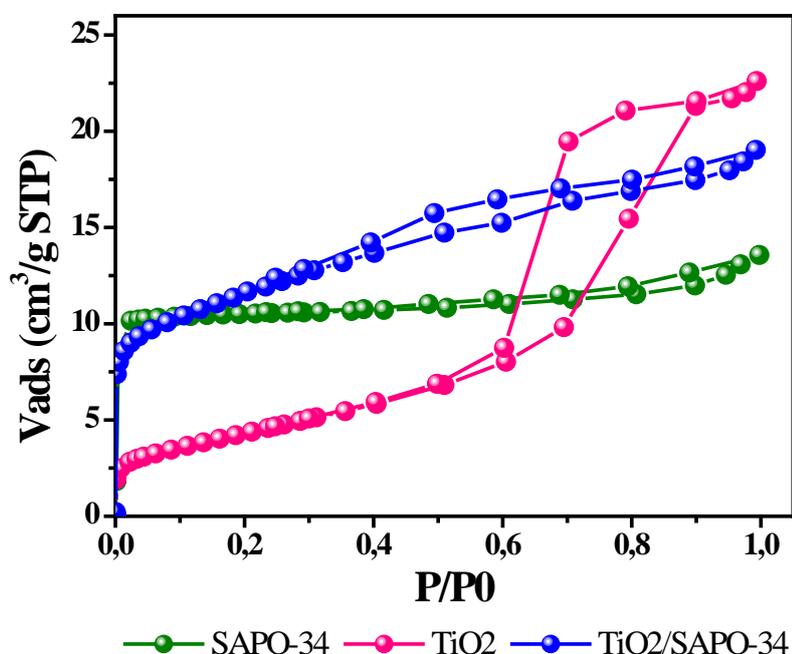

Fig.4. Nitrogen adsorption–desorption isotherms of TiO_2, as-synthesized SAPO-34 and TiO_2/SAPO-34 using as-synthesized SAPO-34 as supports.

Table.1: Textural properties of TiO_2, SAPO-34 and the TiO_2/SAPO-34 composite.

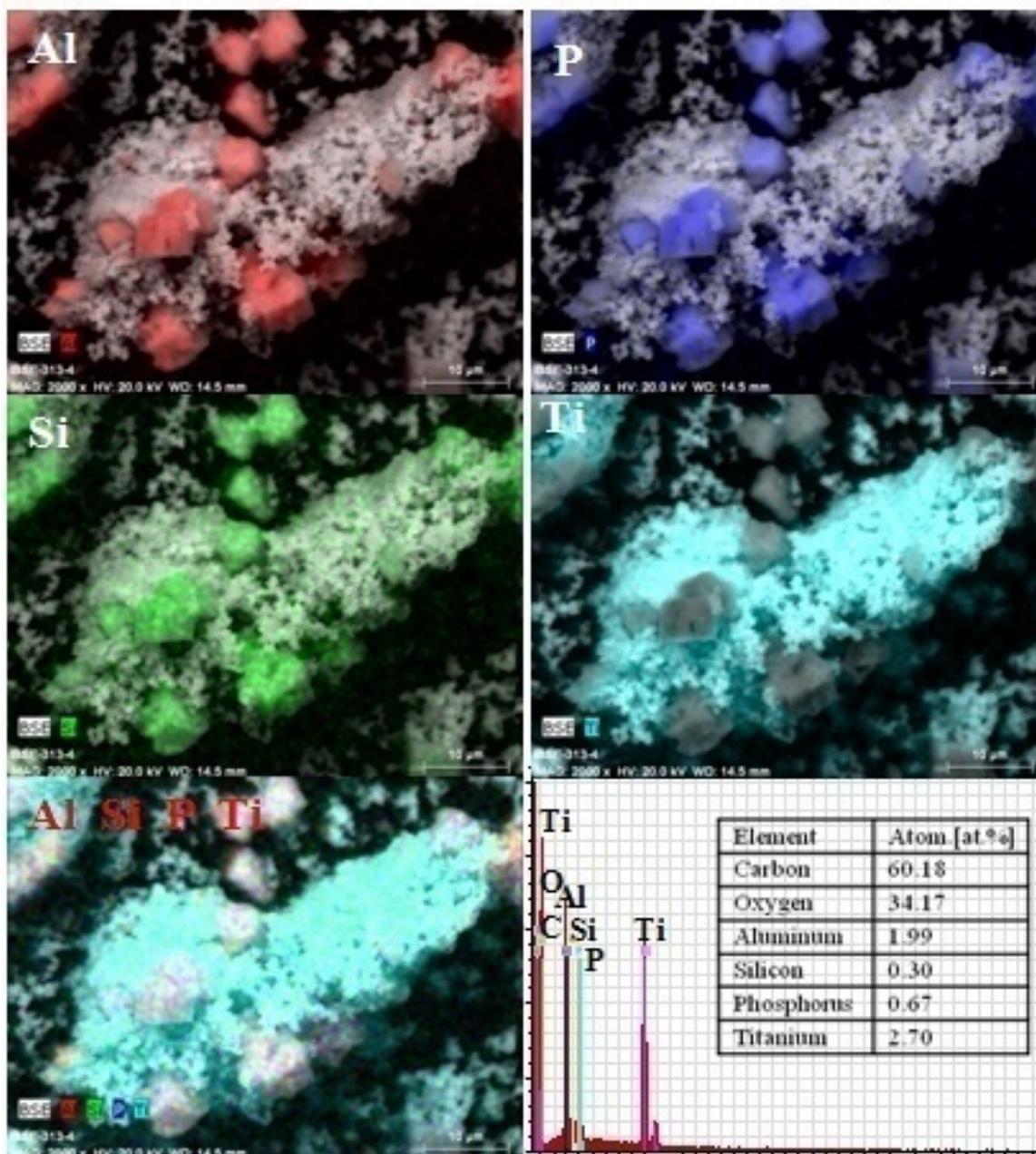| Sample	$S_{BET}(m^2/g)$	$V(Cm^3/g)$	$D_{BJH}(\text{Å})$
SAPO-34	453	0.27	18
TiO_2	83	0.18	90
TiO_2/SAPO-34	295	0.21	30

Fig.5. EDX of TiO$_2$/SAPO-34 prepared by as-synthesized SAPO-34 support.

Fig 5 shows EDX mapping images for the composite TiO$_2$/SAPO-34. According to the chemical composition for the synthesis of TiO$_2$/SAPO-34 we have used the same proportion of TiO$_2$ and the as-synthesized zeolite support (50%). This also shows that the use of the calcination temperature at 400 °C promotes the formation of anatase although the removal of morpholine is partial; The EDX analysis shows that high amount of carbon is obtained confirming that calcination at 400 °C leads to the partial removal of template; these results are in agreement with the TGA analysis. The analysis also shows that titanium is the major element with an atomic percentage of 2.7% and 2% aluminum.
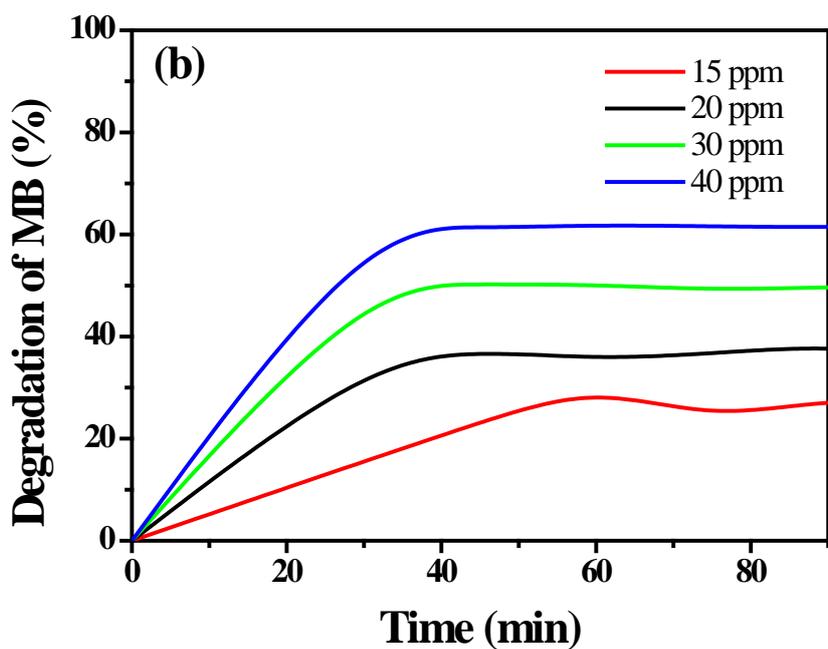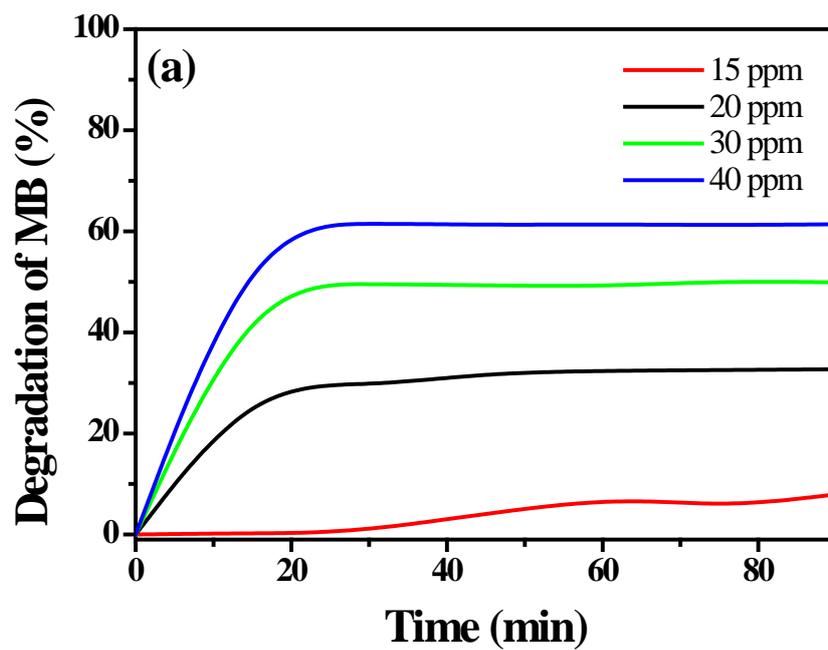
Fig.6. Kinetics of catalytic degradation of methylene blue; (a) in presence of TiO_2 and (b) TiO_2/SAPO-34 nanocomposites.
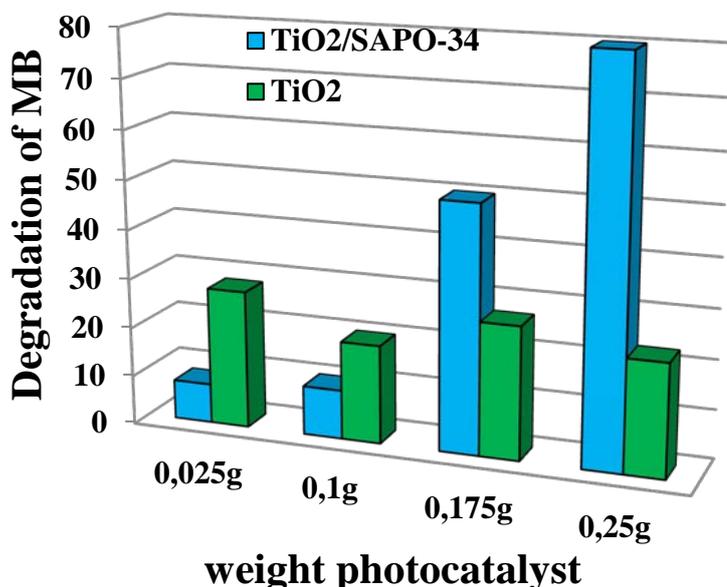
Fig.7. Effect of catalyst mass on MB degradation.

In this part a comparative study between TiO_2 anatase and TiO_2/SAPO-34 composite synthesized by the same method were used as photocatalysts for MB degradation. Knowing that TiO_2 anatase used by the present synthesis method shown significant photocatalytic properties compared to the TiO_2-P25 [46].

The photo-degradation of methylene blue (MB) by TiO_2 and TiO_2/SAPO-34 under visible light are presented in Fig.6 (a and b). The results clearly indicate that the photo-degradation of TiO_2/SAPO-34 sample can reach to 65% (at 40 ppm of MB).The same results are obtained by using TiO_2 after 90 min under UV light irradiation. The equilibrium time is estimated to be about 20 min and 40 min for TiO_2 and composite TiO_2/SAPO-34, respectively, which is due to the low amount of TiO_2 in the composite TiO_2/SAPO-34 (50% TiO_2 and 50% SAPO-34).

This difference is probably due to the content of TiO_2 containing composite. For TiO_2 anatase we used a mass of 0.025g, while in the case of TiO_2/SAPO-34 we have used the same mass that contains 50% TiO_2 Wt. This difference may also be due to the presence of carbon of decomposed template (high amount of carbon, see EDX and TGA results) on the surface which blocks the active sites of TiO_2/SAPO-34 composite material.

We have also studied the effect of MB concentration by varying the dye concentration in the range from 15–40 ppm. As shown in Fig.6, the degradation of MB increases with increasing amounts of MB in solution. At low concentration (15ppm), MB degraded partially while the degradation efficiency of TiO_2/SAPO-34 was found to be increased when the concentration was increased up to 40 ppm. This behavior can be explained on the basis of change in optical density of the MB solution at varying concentration [54]. The density of solution increases with the increase in the MB concentration in solution which restricts the penetration of the light into the solution. We note that the degradation of MB is almost the same for both photocatalysts, knowing that the composite material contains 50% of TiO_2 in the structure compared with the pure TiO_2 (100%).

Fig 7 shows the effect of the catalyst mass on the degradation of MB. We observe that the concentration of dye in the solution decreases with the increase in the mass of TiO_2 up to a certain level and then starts to decrease with a further increase in the catalyst amount. This observation can be explained on the basis of the fact that the number of active sites and the number of absorbed photons increase with the increase in the catalyst amount which causes a higher rate of photocatalysis. After a certain point, light scattering and aggregation of the catalyst particles may occur. This results in the decrease in the photocatalytic performance due to the decrease in the number of active sites in the agglomerated catalyst even as the amount of catalyst is increased [55,56]. Interestingly, the degradation of MB increased with the increase of the mass of the TiO_2/SAPO-34 composite, reaching a degradation of 80% of MB using 0.25 g of TiO_2/SAPO-34 catalyst after 90 min of reaction time. In this respect, it would appear that supporting the TiO_2 on the SAPO-34 support has the clear advantage of preventing the decrease in active sites of the photocatalyst, which may be attributed to the prevention of aggregation of the TiO_2. Furthermore, it must be noted that recoverability of the catalysts was greatly improved in the case of the composite, due to the high density of the SAPO-34 phase, which greatly simplified the filtering of the suspended photocatalyst.

In order to confirm the obtained results between both photocatalysts we have used UV-vis spectroscopy to quantify the light absorption and determine the wavelength range for absorption. As shown in Fig.8. The band gap energy of TiO_2 anatase is found to be 2.9 eV which is equivalent to the wavelength of 423 nm. In regards to TiO_2/SAPO-34 composite showed absorbance in the visible range and its band gap energy is 2.56

eV for wavelength of 479 nm, which suggests its potential to be activated by visible light. It also shows that the narrow band gap benefits the generation of more photoinduced electrons and holes to enhance the photocatalytic activity of composite TiO_2/SAPO-34.
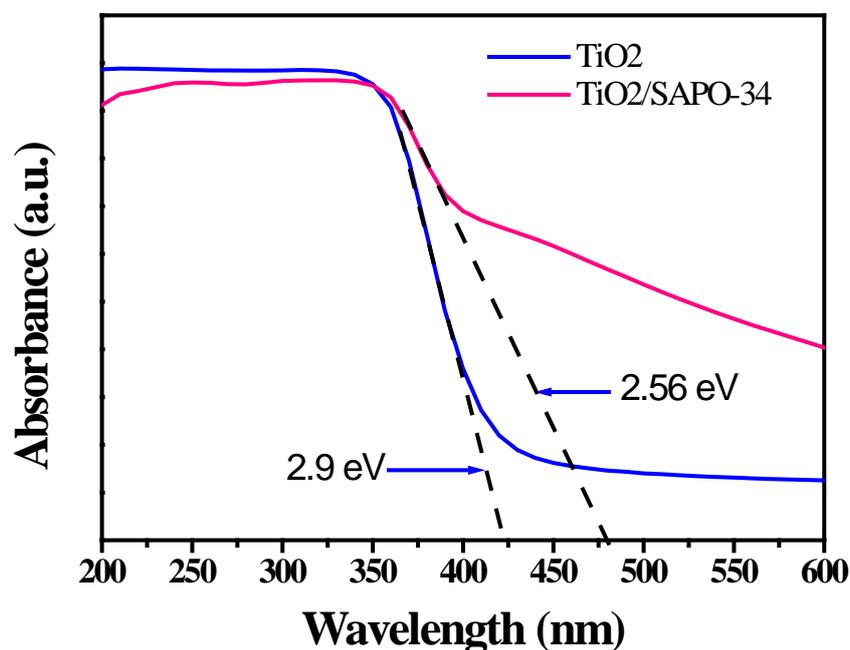

Fig.8. UV–Visible spectra of TiO_2 and composite TiO_2/SAPO-34 obtained by as-synthesized SAPO-34

Conclusions

Three different materials, SAPO-34, TiO_2 and TiO_2/SAPO-34 composite were successfully synthesized and characterized. We have shown that the use of calcined SAPO-34 zeolite as a support for TiO_2 leads a total collapse of the zeolite framework after treatment by calcination at 400°C, providing only one nano-spherical phase characteristic of TiO_2 anatase. The use of as-synthesized zeolite as support results in a phase mixture between TiO_2 anatase and cubic structure of SAPO-34 zeolite. The TGA curves show that the stability of the composite TiO_2/SAPO-34 has been improved compared to TiO_2 pure.

The obtained results revealed the possibility to have a supported TiO_2 catalyst which performs better than TiO_2 for organic dyes degradation in aqueous solution. In addition, TiO_2/SAPO-34 catalysts can be easily recovered once the photocatalytic reaction is finished because of the higher density of SAPO-34 particles. Particularly, TiO_2/SAPO-34 catalysts prepared by sol–gel method exhibited higher activity than TiO_2 in the photodegradation of methylene blue. Catalysts activity is due to the well-dispersed TiO_2 nanoparticles on the

surface of SAPO-34, which induces a synergy effect between both materials that reduces the recombination rate of the electron–hole pair.

References

[1] S. Ananthakumar, J. Ramkumar, S. Moorthy Babu, Renewable and Sustainable Energy Reviews. **57**, 1307–1321 (2016)

[2] R. Mohini, N. Lakshminarasimhan, Materials Research Bulletin. **76,** 370–375 (2016).

[3] Yuan Chunmiao, Paul R. Amyotte, Md. Nur Hossain, Chang Li, Journal of Hazardous Materials. **274**, 322–330 (2014)

[4] M. Hofer, D. Penner, Journal of the European Ceramic Society. **31**, 2887–2896 (2011)

[5] Laxman Singh, Ill Won Kim, Byung Cheol Sin, Sang Kook Woo, Seung Ho Hyunc, Kam Deo Mandal, Youngil Lee, Powder Technology. **280**, 256–265 (2015)

[6] Charline M. Malengreauxa, Sophie L. Pirarda, John R. Bartlettb, c, Benoît Heinrichs, Chemical Engineering Journal. **245**, 180–190 (2014)

[7] A. O. Kondrakov, A. N. Ignatev, F. H. Frimmel, S. Bräsec, H. Horn, A. I. Revelsky, Applied Catalysis B: Environmental. **160–161**, 106–114 (2014)

[8] Zuo-Bin Qin, Liang Tan, Zhao-Qing Liu, Shuang Chen, Ji-Hua Qin, Jie-Jian Tang, Nan Li, Advanced Powder Technology. **27**, 299–304 (2016)

[9] Swati Sood, Surinder Kumar Mehta, A.S.K. Sinha, Sushil Kumar Kansal, Chemical Engineering Journal. 290, Pages 45–52 (2016)

[10] Huihui Wang, Li Ma, Mengyu Gan, Tao Zhou, Xiaowu Sun, Wenqin Dai, Huining Wang, Shiyong Wang, Composites Part B: Engineering. **92**, 405–412 (2016)

[11] Zohre Taghizadeh-Tabari, Saeed Zeinali Heris, Maryam Moradi, Mostafa Kahani, Renewable and Sustainable Energy Reviews. **58**, 1318–1326 (2016)

[12] E. Bet-moushoul, Y. Mansourpanah, Kh. Farhadi, M. Tabatabaei, Chemical Engineering Journal. **283**, 29–46 (2016)

[13] L. B. Arruda, C. M. Santos, M. O. Orlandi, W. H. Schreiner, P. N. Lisboa-Filho, Ceramics International. **41**, 2884–2891(2015)

[14] M. Motlak, N. A. M. Barakat, M. S. Akhtar, A. G. El-Deen, M. Obaid, C. S. Kim, K. A. Khalil, A. A. Almajid, Chemical Engineering Journal. **268**, 153–161(2015)

[15] Alamgir, W. Khan, S. Ahmad, A. H. Naqvi, Materials Letters. **133**, 28–31 (2014)

[16] R. Wang, D. Ren, S. Xia, Y. Zhang, J. Zhao, J. Hazard. Mater. **169**, 926–932 (2009)

[17] C.C. Wang, C.K. Lee, M.D. Lyu, L.C. Juang, Dyes Pigments. **76,** 817–824 (2008)

[18] E. Bet-moushoul, Y. Mansourpanah, Kh. Farhadi, M. Tabatabaei, Chemical Engineering Journal. **283**, 29–46 (2016)

[19] M. M. Momeni, Z. Nazari, Ceramics International. **42**, 8691–8697 (2016)

[20] M. M. Momeni, Y. Ghayeb, Ceramics International. **42**, 7014–7022 (2016)

[21] Xu Song, Yun Hu, Mengmeng Zheng, Chaohai Wei, Applied Catalysis B: Environmental. **182**, 587–597 (2016)

[22] Shahzad Abu Bakar, Caue Ribeiro, Applied Surface Science. **377**, 121–133 (2016)

[23] M.V. Landau, L. Vradman, Xueguang Wang, L. Titelman, Microporous and Mesoporous Materials. **78**, 117–129 (2005)

[24] Y. Gazal, C. Dublanche-Tixier, C. Chazelas, M. Colas, P. Carles, P. Tristant, Thin Solid Films. **600**, 43–52 (2016)

[25] J. Sun, L. Qiao, S. Sun, G. Wang, J. Hazard. Mater. 155, 312–319 (2008)

[26] U.G. Akpan, B.H. Hameed. Applied Catalysis A: General. **375**, 1–11 (2010)

[27] N. Pronina, D. Klauson, A. Moiseev, J. Deubener, M. Krichevskaya, Applied Catalysis B: Environmental. **178**, 117–123 (2015)

[28] I. Pavlovska, K. Malnieks, G. Mezinskis, L. Bidermanis, M. Karpe, Surface and Coatings Technology. **258**, 206–210 (2014)

[29] H. Toiserkani, Progress in Organic Coatings. **88**, 17–22 (2015)

[30] K. Rajendran, V. Senthil Kumar, K. Anitha Rani, Optik-International Journal for Light and Electron Optics, **125**, 1993–1996 (2014)

[31] M. Lafjah, F. Djafri, A. Bengueddach, N. Keller, V. Keller, Journal of Hazardous Materials. **186**, 1218–1225 (2011)

[32] S. Gomez, C. Leal Marchena, L. Pizzio, L. Pierella, Journal of Hazardous Materials. **258–259**, 19–26 (2013)

[33] S. Gomez, C. Leal Marchena, M. S. Renzini, L. Pizzio, L. Pierella, Applied Catalysis B: Environmental. **162**, 167–173 (2015)

[34] M. Takeuchi, M. Hidaka, M. Anpo, Journal of Hazardous Materials. **237–238**, 133–139 (2012)

[35] F. F. de Brites-Nóbrega, A. N. B. Polo, A. M. Benedetti, M. M. D. Leão, V. Slusarski-Santana, N. R. C. Fernandes-Machado, Journal of Hazardous Materials. **263**, 61– 66 (2013)

[36] D. Kanakaraju, J. Kockler, C. A. Motti, B. D. Glass, M. Oelgemöller, Applied Catalysis B: Environmental. **166-167**, 45-55 (2015)

[37] Q. Sun, X. Hu, S. Zheng, Z. Sun, S. Liu, H. Li, Powder Technology. **274**, 88–97 (2015)

[38] V. A. Drebushchak, S. N. Dementiev, Y. V. Seryotkin , J Therm Anal Calorim. **107**, 1293–1299 (2012)

[39] R. Arletti, E. Mazzucato, G. Vezzalini, Am Mineral. **91**, 628–634 (2006)

[40] R. Szostak. Molecular Sieves-Principles of Synthesis and Identification, Van Nostr and Reinhold New York NY (1989)

[41] J. Ma, Z. Si, D. Weng, X. Wu, Y. Ma, Chemical Engineering Journal. **267**, 191–200(2015)

[42] M. Sedighi, J. Towfighi, Fuel. **153**, 382–392 (2015)

[43] M. Masoudi-Nejad, S. Fatemi, Journal of Industrial and Engineering Chemistry. **20**, 4045–4053 (2014)

[44] J. Gong, C. Wang, C. Zeng, L. Zhang, Microporous and Mesoporous Materials. **221**, 128–136 (2016)

[45] A. M. Prakash, S. Unnikrishnan, J Chem Soc Faraday Trans. **90**, 229 (1994)

[46] R. Velmurugan, B. Krishnakumar, R. Kumar, M. Swaminathan, Arabian Journal of Chemistry. **5**, 447–452 (2012)

[47] S. Suárez, M. Yates, P. Avila, J. Blanco, J Catal Today. **105**, 499–506 (2005)

[48] T. Fjermestad, S. Svelle, O. Swang, J Phys Chem C. **117**, 13442–13451 (2013)

[49] A. Buchholz, W. Wang, A. Arnold, M. Xu, M. Hunger, Microporous and Mesoporous Materials. 57, 157–168 (2003)

[50] M. Briend, R. Vomscheid, M. Peltre, P. Man, D. Barthomeuf , J Phys Chem. **99**, 8270–8276 (1995)

[51] Chan Wang, Miao Yang, Peng Tian, Shutao Xu, Yue Yang, Dehua Wang, Yangyang Yuan, Zhongmin Liu. **J. Mater. Chem. A**, **3**, 5608-5616 (2015)

[52] Dehua Wang Peng Tian, Dong Fan, Miao Yang, Beibei Gao, Yuyan Qiao, Chan Wang, Zhongmin Liu. Journal of Colloid and Interface Science. **445**, 119–126(2015)

[53] F. Rouquerol, J. Rouquerol, K. Sing, Adsorption by Powders and Porous Solids, Academic Press, San Diego, USA (1999)

[54] L. B. Reutergardh, M. Iangphasuk, Chemosphere. **35**, 585–596 (1997)

[55] S, Senthilkumaar, K. Porkodi, R. Gomathi, A. Geetha Maheswari, N. Manonmani, Dyes Pigm. **69**, 22–30 (2006)

[56] H. Huang, D. Y. C. Leung, P. C. W. Kwong, J. Xiong, L. Zhang, Catal Today. **201**, 189–194 (2013)